Published in final edited form as:
J Biomed Mater Res A. 2012 May ; 100(5): 1256–1268. doi:10.1002/jbm.a.34012.

Cutaneous and inflammatory response to long-term percutaneous implants of sphere-templated porous/solid poly(HEMA) and silicone in Mice

Philip Fleckman[*,1], **Marcia Usui**[*,1], **Ge Zhao**[1], **Robert Underwood**[1], **Max Maginness**[2], **Andrew Marshall**[2], **Christine Glaister**[2], **Buddy Ratner**[3], and **John Olerud**[1]

[1]Dermatology, University of Washington, Seattle, WA

[2]Healionics, University of Washington, Seattle, WA

[3]Depts of Bioengineering and Chemical Engineering, University of Washington, Seattle, WA

Abstract

This study investigates mouse cutaneous responses to long-term percutaneously implanted rods surrounded by sphere-templated porous biomaterials engineered to mimic medical devices surrounded by a porous cuff. We hypothesized that keratinocytes would migrate through the pores and stop, permigrate, or marsupialize along the porous/solid interface. Porous/solid-core poly(2-hydroxyethyl methacrylate) [poly(HEMA)] and silicone rods were implanted in mice for 14 days, 1 month, 3 months, and 6 months. Implants with surrounding tissue were analyzed (immuno)histochemically by light microscopy. Poly(HEMA)/skin implants yielded better morphologic data than silicone implants. Keratinocytes at the poly(HEMA) interface migrated in two different directions. “Ventral” keratinocytes contiguous with the dermal-epidermal junction migrated into the outermost pores, forming an integrated collar surrounding the rods. ”Dorsal” keratinocytes appearing to emanate from the differentiated epithelial layer, extended upward along and into the exterior portion of the rod, forming an integrated sheath. Leukocytes persisted in poly(HEMA) and silicone pores for the duration of the study. Vascular and collagen networks within the poly(HEMA) pores matured as a function of time up to 3 months implantation. Nerves were not observed within the pores. Poly(HEMA) underwent morphological changes by 6 months of implantation. Marsupialization, foreign body encapsulation and infection were not observed in any implants.

INTRODUCTION

The use of percutaneous medical devices has become common place in medical care. Access through the skin to vessels, body cavities, subcutaneous tissue and bone affords diagnostic and therapeutic advantages. However, percutaneous devices are at risk of infection and implant instability. A potential solution is to biointegrate the skin directly with such devices. It has been shown that appropriate porosity encourages cutaneous incorporation (reviewed in Fleckman, 2008).[1] In previous studies using a mouse model, we demonstrated cutaneous incorporation into sphere-templated, porous poly(2-hydroxyethyl methacrylate) [poly(HEMA)] with precisely controlled uniform pore diameters (40 μm) and uniform inter-connecting throats (~16 μm). Implants remained in place for 28 days without signs of infection or loss of implant integrity.[2] In this study poly(HEMA) and silicone rods were engineered using either poly(HEMA) or silicone with a nonporous (solid) circular core

[*]these authors contributed equally

surrounded by a sphere-templated porous outer layer with 36-μm diameter pores and ~14-μm interconnecting throats [porous/solid poly(HEMA), or porous/solid silicone]. This design was chosen to mimic a solid device surrounded by a porous cuff (e.g. catheters, prosthetic attachment sites). We then asked the questions: 1) what is the cutaneous response at the porous/solid interface, and 2) what is the long-term cutaneous response to these implants in the mouse model. Poly(HEMA), a hydrogel that has favorable swelling and mechanical properties facilitates tissue/implant sectioning, histological staining and morphological assessment.[2–5] Silicone, although difficult to section and stain, was selected since many percutaneous medical devices are made of silicone. We hypothesized that keratinocytes would migrate through the pores, eventually reach the solid core and subsequently stop, permigrate, or marsupialize along the porous/solid interface.

METHODS

Porous implant synthesis

Poly(HEMA)—Porous poly(HEMA) implants with a solid core were produced by infiltrating an initiated monomer solution into porous templates comprised of sintered poly(methyl methacrylate) (PMMA) beads that were sieved to a narrow size distribution. The initiated monomer solution consisted of 0.8 g ammonium persulfate (Sigma-Aldrich, St. Louis, MO), 0.3 g sodium metabisulfate (Sigma-Aldrich) and 4 g endotoxin free water (Thermo Scientific, Pittsburgh, PA) mixed with a monomer solution containing 21.4 g ophthalmic grade hydroxyethylmethacrylate (Polysciences, Warrington, PA), 6.8 g ethylene glycol (Sigma-Aldrich), and 0.995 g tetraethylene glycol dimethacrylate (Sigma-Aldrich) and 4 g endotoxin-free water (Thermo Scientific). The initiated monomer solution was infiltrated into templates that contained a hollow core. The PMMA templates were then completely covered with the solution, put in a sealed container and polymerized at room temperature for 24 hours. The template material was then solubilized out with dichloromethane, resulting in a porous structure with a solid rod in the center. The resulting cylindrical implants were approximately 10 mm long and 1.2 mm in diameter, with a solid core measuring 0.4 mm in diameter surrounded by porous poly(HEMA) with pores measuring approximately 36 μm in diameter and interconnecting throats measuring 14 μm. The implants were packaged in vials with phosphate buffered saline and autoclave sterilized.

Silicone—Porous silicone implants were produced by infiltrating a cylindrical PMMA template that contained a solid core with premixed parts A and B of MED-4211 silicone (Nusil) and curing at 75°C for 16 hours. The template material was then solubilized out, resulting in a porous structure with a hollow core. These porous cylinders were then mounted on (stretched over) solid silicone (MED-4211) rods. The solid core measured approximately 0.4 mm in diameter by 10 mm long. The final cylindrical implants with the surrounding porous silicone with pores measuring approximately 36 μm in diameter, with interconnecting throats measuring ~14 μm were 1.2 mm in diameter (the solid rod extending a few millimeters beyond the outer porous region). The implants were packaged in vials with phosphate buffered saline and autoclave sterilized.

These materials were provided by Healionics, Inc. who hold the patent on the sphere-templated engineering process [US Patent 7,972,628 (Ratner/Marshall) for more details].

Mouse Implantation

Animal studies were conducted with University of Washington Institutional Animal Care and Use Committee approval in compliance with the NIH Guide for the Care and Use of Laboratory Animals, 1996. Eight-week-old female C57BL/6 mice (Jackson Laboratory, Bar Harbor, ME) were housed five mice per cage prior to surgery and individually housed post-

implant procedure in a temperature-controlled animal facility. A total of 32 mice were used for the study. Mice were anesthetized and the dorsal skin was shaved, treated with depilatory cream (1.5 min), wiped with warm moistened gauze, and cleansed with 10% povidone-iodine followed by an alcohol wipe. A 14-gauge needle was used to pierce the skin in a through-and-through fashion, creating two wound (exit) sites 0.5 cm apart midline between the scapulae and 1 cm posterior to the ears. The rod-shaped implant was placed in the lumen of the needle and the needle was withdrawn, leaving the porous rod implanted through the skin with the two ends of the rod extending from two exit sites. A second rod was placed 1 cm caudal to the first implant via the same technique. Each mouse was implanted with 1 porous/solid poly(HEMA) rod and 1 porous/solid silicone rod with regional implantation site alternated. Animals were placed on a heating pad following surgery and allowed to recover fully from anesthesia before caging.

Macrophotography and image analysis

Macrophotographs of the mice with an adjacent ruler were taken using a Canon G11 digital camera. Comparative photographs of mice at the time of implant and harvest were normalized to ruler scale. The length between the two exit sites of the upper region directly above the implanted biomaterial, referred to as the “bridge” of skin, was measured at the time of implant and time of harvest. The percent change in measurements of harvest measurement/implant measurement of the “bridge” of skin was then tabulated as a function of implant time.

Tissue Harvest

Mice were euthanized with a lethal dose of intraperitoneal pentobarbital. Implants and surrounding skin were harvested at 14 days and at 1, 3 and 6 months after implantation. The entire region containing the two biomaterial implants was excised *en bloc* from the back of each mouse down to the level of the deep fascia. Each implant with surrounding skin was then separated from the larger excision specimen using dissection scissors and scalpel. Implant specimens were then either frozen in O.C.T. (Sakura Finetek Inc., Torrance, CA) for (immuno)histochemistry or bisected between the 2 exit sites, fixed in half strength Karnovsky’s[6], and processed for Poly/Bed® 812 resin (Polysciences Inc., Warrington, PA) embedding for electron microscopy as previously described.[4] Semithin sections, 1 μm in thickness, were stained with Richardson’s stain[7] for examination using light microscopy.

The experiment was designed to investigate both poly(HEMA) and silicone implants by gross clinical observations and by light and electron microscopic tissue analysis. Of the 32 mice implanted with rods, 24 of the mice were designated for light microscopic studies and 8 mice were designated for electron microscopy. Tissue sections of the porous/solid poly(HEMA) and porous/solid silicone (6 rods/time point) were evaluated for cutaneous and inflammatory response.

Histology and Immunohistochemistry

Poly(HEMA)—Duplicate 6-μm frozen poly(HEMA)/skin sections were stained with hematoxylin and eosin (H&E) for histology and with picrosirius red [Direct red 80 (Sigma-Aldrich)] for the presence of collagen. Sections were immunolabeled using routine immunoperoxidase methods as previously described in Fukano et al., 2006.[4] Brievly, tissue sections were fixed in cold acetone prior to immunolabeling. Primary antibodies used were: pooled pankeratin (rabbit, 1:1000, Dako, Carpenteria, CA)/keratin 14 (rabbit, 1:1000, Covance, Princeton, NJ), pan-macrophage/monocyte marker F4/80 (rat, 1:50, MCA519G, SeroTec, Raleigh, NC), platelet/endothelial cell adhesion molecule-1 (PECAM-1 or CD-31) (rat, 1:500, Research Diagnostics, Concord, MA), and neurofilament (rabbit, 1:3000, Sigma, St. Louis, MO). Secondary antibodies used were biotinylated donkey anti-rat (1:1600,

Jackson ImmunoResearch, West Grove, PA) or biotinylated goat anti-rabbit (1:200, Vector Laboratories, Burlingame, CA). Following secondary antibody labeling, sections were incubated with strept-avidin-biotin complex [1:50, Vectastain Elite ABC kit (peroxidase), Vector Laboratories, Burlingame, CA], with 0.12% 3,3'-diaminobenzidine used as chromogen. Glycergel (Dako, Carpenteria, CA) was used as mounting media.

Silicone—Twelve-micron frozen silicone/skin sections were H&E stained with a modified protocol. In standard H&E staining[8], following the staining step with eosin, tissue samples are dehydrated through a series of graded ethanol and further dehydrated using solvents such as xylene or Histoclear. Silicone tissue sections were rinsed in distilled water following eosin staining. Water was gently wicked from the sections using filter paper and sections were then directly coverslipped using Glycergel for mounting media. Ethanol and dehydrating solvents such as xylene or Histoclear were not used since they cause silicone to swell. Silicone sections were not stained with picrosirius red due to the need to incubate sections in ethanol. Silicone sections were immunolabeled in the same fashion as poly(HEMA) sections with antibodies to pankeratin/K14, F4/80, and PECAM-1 with the exception that fixation in cold acetone prior to immunolabeling was omitted.

Photomicrography

Tissue sections were viewed with a Nikon Microphot-SA microscope and images captured using a Spot Flex color digital camera (Diagnostic Instruments, Sterling Heights, MI) for brightfield, differential interference contrast and polarized light images. Photoshop® (Adobe Systems Inc., San Jose, CA) was used for image color adjustment.

Data analysis

Statistical significance was determined by using one-way ANOVA and two-sided Student's *t*-test. The significance level was set at $\alpha=0.05$.

RESULTS

Clinical Observations of Implanted Mice

Examples of mice at the time of rod implantation and the time of harvest are seen in Figure 1. Clinical signs of irritation or infection were not seen. One mouse with malocclusion of its teeth did not survive.

Skin contraction between exit sites—Measurements of the length of the skin bridge above the implant were made as indicated by the yellow dotted lines in Figure 2. These measurements were made from the gross images taken at time of implant and time at harvest. The 14 day data was not included as hair growth precluded measurement and 3 mice from the 3 month harvest could not be evaluated due to mechanical problems with image capture. Results are depicted in the graph for 1, 3 and 6 month implantations with 8, 5, and 4 mice evaluated for poly(HEMA) implants and 8, 5, and 7 mice evaluated for silicone implants, respectively. The percent change in length of the skin bridge at time of harvest for both porous/solid poly(HEMA) and porous/solid silicone implants was calculated by dividing the distance between exit sites at time of harvest by the distance between exit sites at time of implantation. An average of the distances for each harvest time point was taken and standard error calculated for the averaged data (Figure 2). Contraction of the upper bridge region of the skin was greater for silicone implants than for the poly(HEMA) implants.

Gross observations of implant integrity—Table 1 shows implant integrity for both poly(HEMA) and silicone for all time points. Each exit site of the implants was evaluated

separately (1 implant = 2 exits sites). Evaluations of implants were made of 8 mice at 14 days, 8 mice at 1 month, 5 mice at 3 months and 7 mice at 6 months. Three mice from the 3 month harvest could not be evaluated due to loss of data as the result of mechanical problems with image capture.

The exposed regions of the implanted poly(HEMA), which was hydrated in phosphate buffered saline until implantation, dried out over time and became brittle by 3 months. In many cases, this resulted in the external portion of the implants breaking off. Some of the exit sites were completely covered by skin by 6 months (Table 1). The silicone implants remained intact *in situ* in all but one of the implants (Table 1). The outer porous silicone region appeared to separate from the solid core at many of the exit sites.

Histology

Poly(HEMA) and silicone implants with surrounding tissue from 6 mice at 14-day and at 1-month and 3-month time points and 5 mice from the 6-month time point were studied. An illustration depicting the implant orientation and general morphology is shown in Figure 3. Occasionally, imperfections or breaks within the solid portion of poly(HEMA) were seen within the solid central core and were termed “voids”. Voids contiguous with the porous region were seen in tissue sections of 4/6 rods at 14 days post-implantation, 3/5 rods at 1 month (1 implant lost at time of sectioning), 2/6 rods at 3 months, and 4/4 rods (1 implant missing in sample) at 6 months. Voids contiguous with the surrounding porous material were filled with cells and matrix. A scanning electron micrograph is included in Figure 3, showing the porous/solid poly(HEMA) interface with potential areas of voids in the solid poly(HEMA) regions illustrated in the cartoon. Difficulty in sectioning silicone[3] compromised histological analysis of intact tissue/rod sections. The silicone solid core separated from the outer porous silicone region during cryosectioning for all but one sample.

Morphological analysis of the poly(HEMA) implants yielded better quality data and more consistent results than morphologic data from the silicone implants.

Poly(HEMA)

Epidermis—Epidermal incorporation was seen at all time points in the specimens in which the epidermal/implant region was retained. At the implant interface, the epidermis appeared to bifurcate and migrate in two directions, resulting in two populations of keratinocytes migrating into the pores at all times of implantation. Keratinocytes contiguous with the original dermal epidermal junction (ventral keratinocytes) migrated a short distance down the implant and into the pores of the implant. The second population of keratinocytes appeared to emanate from the suprabasal layers of the epidermis (dorsal keratinocytes) and migrated upward along and into the implant, forming a sheath-like structure around and into the exterior portion of the implant (Figures 4 a–d). Sheaths were seen in sections at all time points, although the brittle exposed poly(HEMA) at the exit sites frequently fractured during sectioning, precluding systematic evaluation. The two populations of keratinocytes migrated quite differently. Migration distance of keratinocytes from the ventral collar of keratinocytes was limited at 14 days and appeared to be less in the1 month implants (arrowheads in Figure 4 e–l). Keratinocytes in the 3-month and 6-month implants appeared to form a blunt, non-migrating tongue. Keratinocytes that appeared to emanate from the dorsal aspect of the epidermis appeared to migrate farther, especially in the 3-month implants and filled adjacent pores with cornified cells. Cornified cells at the implant/epidermal region were found within the pores as early as 14 days post-implantation and appeared to become more hyperplastic as a function of time. (Figure 4 e–h asterisks). Neither ventral nor dorsal layer keratinocytes marsupialized at the porous/solid interface, and there was no evidence of keratinocytes migrating down through the pores containing dermal structures.

Dermis—Endothelial cells, identified by PECAM-1 staining, were present at all time points (Figure 5 a–d). Figures 5 a–d represent the central region of the rod between the two exit sites. Both the number and branching of vessels between pores increased as a function of time up to 3 months, but appeared to be reduced in the 6-month implants. In contrast, vessels in the pores adjacent to the exit sites remained large and viable, as indicated by presence of red blood cells in the 6-month implants. Vessels were seen within the voids in the solid core that were contiguous with the surrounding porous material (Figure 5 e–h). The vessels seen in the voids of 6-month implants remained large and viable. Nerves, identified by the neurofilament antibody, were not seen within the implant pores or voids (not shown).

Picrosirius red stain, visualized using polarized light, was used to identify collagen deposition within the pores. Immature fibers in the figure appear green using polarization, while thicker, more robust fibers appear yellow to red. Collagen thickness in the implants (Figure 5 i–l) increased as a function of time up to 3 months and then decreased in thickness in the central region of the rod between the two exit sites. Collagen in the pores adjacent to the exit sites remained robust throughout all time points. Very thick collagen bundles were seen in voids within the solid cores of implants at all time points (Figure 5 m–p).

Semi-thin (1-μm) sections of Poly/Bed® embedded poly(HEMA) rods showed better retention of cellular morphology. In the Richardson's stained sections, collagen was seen in close juxtaposition with fibroblasts (identified strictly by morphology) in the micro-niches of the pores in the 14-day to 6-month implants with some fibroblasts in the 3-month implants appearing to be vacuolated within the pores [Figure 6 a–d, black arrows (non-vacuolated), red arrow (vacuolated)]. In the tissue surrounding the 1-month to 6-month implants both non-vacuolated and vacuolated fibroblasts were seen [Figure 6 e–h black arrows (non-vacuolated), red arrows (vacuolated)]. Since the pores of the 6-month implants were filled with vacuolated cells (Figure 6 d), it was difficult to determine by light microscopy whether the cells were fibroblasts or macrophages. Very little collagen was seen in pores in the central regions of the implants of the 6-month implants.

Inflammatory response—Acute inflammatory cells (primarily polymorphonuclear leukocytes, identified by multi-lobed nuclei in H&E stained sections) formed within the pores at exit sites and remained as late as 6 months after implantation in the implants in which the epidermal/implant region was retained (Figure 7 a–d).

At all time points, macrophages, identified by immunostaining with an F4/80 antibody, were found within pores throughout the implants (Figure 7 e–l). Immunostained cells appeared to line the surface of pores found at the exit sites and in the region of the dermis of the 14-day implants (Figure 7 i). The staining of macrophages in the 1- and 3-month implants appeared to be more homogeneous (Figure 7 j, k), filling most of the pores, and the staining in the 6-month specimens appeared to be more heterogeneous (Figure 7 l). The Richardson's stained 1-μm sections showed greater cellular detail (Figure 7 m–p). By 3 months, the macrophages appeared very bloated. Multinucleated cells appeared to form by 1 month (open arrows in Figure 7 m–p). The cells that occupied the central, porous region of the 6-month implants were very vacuolated (Figure 7 p). Collagen is identified by asterisks in Figure 7 m–p. Macrophages did not appear to line the large voids seen within implant solid cores in the 14 day – 3 month implants (Figure 7 q–s) but could be seen (brown immunoperoxidase stain) in juxtaposition with the wall of the voids in the 6-month implant (Figure 7 t). Dotted lines in Figure 7 q–t depict the edge of the void and solid lines indicate margins of F4/80 staining.

The poly(HEMA) appeared to undergo a physical change with time, as can be seen in Figures 5 d, 7 h, and 7 l. The well-delineated and uniform pores in the 14-day to 3-month specimens appeared to become more amorphous in the 6-month specimens. In addition, the

porous region of the implant appeared to expand with implantation duration, resulting in increased rod diameter. Quantification of the changes in poly(HEMA) diameter would require analysis of implants sectioned in an *en face* orientation rather than the transverse sections analyzed for this study.

Silicone

Epidermis—During sectioning, the external, air-exposed regions of the implants at the exit sites broke off in most samples. Thus, though the exposed silicone was retained in a few sections (Figure 8 b and c), analysis of the outer sheath was limited. A sample of an exit site of silicone implant is shown is Figure 8 d. The epidermis in the silicone implants appeared to respond similarly to the poly(HEMA) implants. Keratinocytes showed limited migration at all time points as seen in Figures 8 e–h for 14 day and 1, 3, and 6 month implants, respectively.

Dermis—Vessels, as identified by PECAM-1 labeling, were seen throughout all time points (Figure 8 i–l, for 14 day and 1, 3, and 6 month implants, respectively). The quality of sections precluded determining if a pattern of vessel formation was dependent on implant duration. Collagen was seen in the H&E sections prior to mounting with Glycergel, however the eosin stain dissipated from the tissue sections once cover-slipped.

Inflammatory response—Monocytes/macrophages, as identified by F4/80, showed a pattern of labeling similar to that of sections of poly(HEMA) (Figure 8 m–p, for 14 day and 1, 3, and 6 month implants, respectively). Multinucleated macrophages were also seen in a few of the silicone implants (Figure 8 o). It was difficult to discern presence of bloated macrophages in the thicker sections required for optimal sectioning of the silicone [12 μm vs. 6 μm for the poly(HEMA)].

DISCUSSION

In this paper we show long-term (up to 6-month) cutaneous biointegration into sphere-templated porous poly(HEMA) and silicone with a central solid core implanted into mice. Cylindrical rods with a central solid core were used in this study to approximate more closely the conformation of percutaneous medical devices with porous cuffs, as might be used in a clinical situation. The sphere-templating process by which uniform pore diameter and interconnecting throat size can be precision-engineered allows the study of cellular and matrix response not confounded by variability of pore size as shown by others.[9, (and references cited therein)] The uniformity of pore and throat size also allows evaluation of the overall pattern of cellular and matrix response throughout the entire implant.

We hypothesized that the epidermis would migrate across the porous portion of the implant and would restore barrier function of the skin by reaching the solid central core. We observed that the epidermis did not migrate through the entire porous portion of the implant at the times studied, but rather displayed a unique ingrowth pattern along and into the porous implants.

In normal wounds without implants, keratinocytes associated with the dermal-epidermal junction (ventral) are traditionally thought to be the primary keratinocytes involved in wound closure. In this implant model, ventral keratinocytes showed limited migration into both poly(HEMA) and silicone implants, as previously quantified by Underwood et al., 2011 for poly(HEMA) rods.[10] In the poly(HEMA) implants, a secondary migrating epidermal layer that appeared to arise from the differentiated layers of the epidermis formed a thick sheath around and into the exposed region of the implant, external to the exit site. The

keratinocytes appeared to migrate up along the implant. We have observed a similar bifurcation of keratinocytes in normal human incisional wounds (unpublished data), with the dorsal keratinocyte layer appearing to be associated with the scab. Since the region of this sheath is the same region in which serum and neutrophils reside, much like a scab, perhaps these upper keratinocytes are interacting with or reacting to a scab-like neutrophilic/serum environment within the pores. The lack of integrity of most silicone implant histological sections precluded similar analysis.

A novel observation of this long-term implant study was the presence of a hyperplastic, cornified epidermal layer of dorsal keratinocytes, both inside the pores and surrounding the implant. With the presence of this layer, one cannot rule out that the skin may be attempting to extrude the implant via keratinocyte differentiation; this process has been described as permigration.[11, 12] Since the implants in our study were through and through, with two exit sites, the counter forces produced by keratinocyte differentiation at both ends of the implants possibly precluded extrusion of the implant but may explain the decrease in size of the 'bridge' portion of the skin. The cornified cells found within the pores may also be a downstream effect of persistent neutrophils at the exit sites. Neutrophils have been shown to promote keratinocyte differentiation.[13]

In normal wounds without implants, keratinocytes migrate a much greater distance (several millimeters) across the wound matrix than was seen in this Implant study and in a study in which epidermal migration was quantified in implanted poly(HEMA) implants.[10] A possible explanation for the decrease in keratinocyte migration is the early and prolonged presence of neutrophils along the region of the epidermis and the massive influx of macrophages that line the interior of the poly(HEMA) pores. Neutrophils are seen only in the initial stages of normal wound healing, followed by an influx of monocyte/macrophages.[14, 15] Persistent neutrophils are seen in chronic, non-healing wounds and are thought to play a role in failure of the keratinocytes to close a wound[16], while wound closure has been shown to be accelerated in neutropenic mice[17]. Neutrophils still present in the 6 month implants may negatively affect keratinocyte migration. In addition, neutrophil-derived proteases are known to degrade extracellular matrix, and this proteolysis could then lead to keratinocyte detachment.[13] Keratinocytes must contact extracellular matrix components for migration and proliferation.[18]

Collagen was seen at, and at times, above the level of the epidermal region at the exit site in the poly(HEMA) pores perhaps limiting keratinocyte migration. Winter suggested that the presence of dermal components limits permigration and marsupialization of keratinocytes.[19]

Vessels matured in the dermal region of the poly(HEMA) implants up to 3 months after implantation. The fact that fewer vessels, as detected by the PECAM-1 antibody, were present in the central portions of 6-month poly(HEMA) implants may be indicative of a return of the tissue to a more normal quiescent "healed" state. In the granulation tissue formation stage of normal wound healing, angiogenesis predominates with an influx of capillaries that eventually anastomose, resulting in fewer and larger vessels necessary to vascularize the tissue. Vessels in the surrounding tissue near the exit sites and in the void regions of the solid core for the 6-month implants appeared to be robust and mature. Too few silicone sections could be evaluated to make a definitive assessment of vessel quantity or distribution pattern, however vessels were seen in the silicone implants at all time points. Since vascular endothelial cells and mast cells present in the pores should provide nerve growth factor necessary for nerve chemotaxis and survival,[20, 21] it is curious that we found no indication of innervation within the dermal region of the poly(HEMA) pores.

The micro-niche of each implant pore provides a unique wound healing environment. Collagen fiber bundles appeared to thicken with implantation time within the poly(HEMA) pores and remained robust up to 3 months implantation. Collagen occupied the central region of each pore, and appeared to traverse each pore through the interconnecting throats as seen in previous studies,[2] while macrophages lined the surfaces of the pores in the incorporated dermal region. Collagen in the 6 month implants was seen in the regions of the exit sites, but decreased in the central portions of the poly(HEMA) implants. Again, the lack of integrity of most silicone implant sections precluded similar analysis.

In the normal progression of cutaneous wound healing, chemoattractant factors such as fibroblast growth factor, platelet derived growth factor, and transforming growth factor β1, produced by platelets, macrophages, and keratinocytes draw fibroblasts into the wound bed.[14] These fibroblasts proliferate, deposit collagen, and undergo apoptosis,[22] while collagen remodeling ensues[14].

We offer a possible explanation for the loss of collagen in the pores of the central portions of the 6-month poly(HEMA) implants. Unlike the normal wound matrix, macrophages persisted and fully lined each pore. Studies have supported a dual nature of macrophages, dependent on the environment in which they reside.[23, 24] In some cases, macrophages assume an aggressive, activated role in fighting infection. These activated macrophages express pro-inflammatory cytokines, chemokines, MHC-II and co-stimulatory molecules, resulting in increased microbicidal activity and tissue destruction. In other environments, macrophages express IL-10 and other cytokines and encourage tissue repair by promoting collagen deposition and vessel. Macrophages in the 3- and 6-month poly(HEMA) implants appeared bloated and were abundant in each pore, leaving little room for blood vessels or collagen to reside in the pore. From these observations, we hypothesize that fibroblasts initially migrated into the pores, deposited collagen, underwent apoptosis[25], and were then phagocytized by macrophages. The foamy (vacuolated) morphology of the macrophages found in the 6-month implants may be indicative of this macrophage activation.[24]

The presence of large voids (100–200 μm in diameter) in the poly(HEMA) solid core, though not intentional features of the implants, revealed an interesting biological response. A previous study comparing sphere-templated poly(HEMA) rods with either 20-, 40-, 60- and 90-μm pore sizes in an *in vitro* rafted organ culture model showed that keratinocytes migrated into the 40- and 60-μm pores but did not migrate into the 90-μm porous rods.[4] Studies of sphere-templated poly(HEMA) suggest maximal vessel incorporation in subcutaneous implants with 35–40 μm pores.[26] These larger voids may retard keratinocyte migration, while vessel development and collagen deposition can still take place. Studies have shown that cell adhesion and activity vary with cell type, biomaterial composition and pore size, thus an optimal pore size may be required for each specific cell type.[9, (and references cited therein)] This would suggest that the geometry of porous-surfaced percutaneous devices may need to be engineered with the appropriate small and/or larger pores to accommodate the biological response desired in a complex environment such as the skin.

All implants in this model remained clinically uninfected. Since the exit sites were not protected from the external environment, the exposed pores could potentially serve as portals for bacteria. The immune system of mice may be very different from humans, as it has been shown in open wound studies that despite the fact that multiple bacteria normally reside on mouse skin under the best of conditions in animal facilities[27], the wounds do not become infected[28–31]. Perhaps a barrier is formed at the implant exit sites, not in the traditional sense by restoration of the epidermal barrier, but by inflammatory cells

positioned in each pore and ready to attack bacteria coursing through a pore. Careful study of this “barrier” zone awaits further investigation.

Limitations

Our results indicate that the poly(HEMA) implants could be morphologically evaluated up to 3 months of implantation, thus this implant mouse model is excellent for studies in this time frame. The shortening of the “bridge” tissue over time could be attributed to permigration in an implant with two exit sites. Alternatively, it is important to keep in mind that since this is a mouse model, the effects of wound contraction must be taken into consideration, especially for long-term studies. Contraction plays a major role in healing of wounded mouse skin,[32] and the shortening of the “bridge” tissue over time may have been due to the contractile forces of myofibroblasts in the surrounding skin[33]. Shortening of the bridge may explain formation of the sheaths if the skin retracted towards the center of each rod. Sheath formation, however was seen in the 14-day implants, while contraction was not seen until 3 months post implantation. Contraction could also play a role in the change in the physical appearance of poly(HEMA) over time. Since poly(HEMA) is a hydrogel, the physical properties of the poly(HEMA) may be subject to these contractile forces. Alternatively, the poly(HEMA) change may reflect chemical alteration in the biomaterial caused by the abundance of activated macrophages and their downstream cytokine expression, or a chemical change in the poly(HEMA) by 6 months implantation. Contraction of the cutaneous bridge between entrance and exit of percutaneous devices was more prominent for the silicone implants and appeared to increase as a function of time; however, the porous geometry of the silicone did not appear to undergo physical changes by 6 months implantation.

Summary

In conclusion, we demonstrate long-term implantation of sphere-templated porous poly(HEMA) and silicone surrounding a solid core in mice in the absence of infection and acute inflammation. Neither marsupialization nor encapsulation (despite the presence of macrophage multinucleated giant cells) was seen in the morphologically evaluated poly(HEMA) implants. This mouse model allows pursuit of studies to determine how cutaneous cells and matrix biointegrate with percutaneous medical devices.

Future studies are needed to evaluate the cutaneous and inflammatory response at the ultrastructural level to further evaluate cellular interaction within the micro-niches of the pores and to develop methods to better retain the material integrity at the exit site.

Acknowledgments

Major funding sources from Washington Technology Center RTD Grant, Healionics Corporation, NIH – NIBIB R01 EB004422, NSF - EEC 9529161 and the George F. Odland Endowed Research Fund. Special thanks to generous support from Dr. Marvin & Judy Young, Dr. John & Darcy Halloran, Dr. Peter Odland, and Dr. Peter Byers.

References

1. Fleckman P, Olerud JE. Models for the histologic study of the skin interface with percutaneous biomaterials. Biomed Mater. 2008; 3 034006.
2. Fukano Y, Usui ML, Underwood RA, Isenhath S, Marshall AJ, Hauch KD, Ratner BD, Olerud JE, Fleckman P. Epidermal and dermal integration into sphere-templated porous poly(2-hydroxyethyl methacrylate) implants in mice. J Biomed Mater Res A. 2010; 94:1172–1186. [PubMed: 20694984]
3. Knowles NG, Miyashita Y, Usui ML, Marshall AJ, Pirrone A, Hauch KD, Ratner BD, Underwood RA, Fleckman P, Olerud JE. A model for studying epithelial attachment and morphology at the

interface between skin and percutaneous devices. J Biomed Mater Res A. 2005; 74:482–488. [PubMed: 15983994]

4. Fukano Y, Knowles NG, Usui ML, Underwood RA, Hauch KD, Marshall AJ, Ratner BD, Giachelli C, Carter WG, Fleckman P, Olerud JE. Characterization of an in vitro model for evaluating the interface between skin and percutaneous biomaterials. Wound Repair Regen. 2006; 14:484–491. [PubMed: 16939578]
5. Isenhath SN, Fukano Y, Usui ML, Underwood RA, Irvin CA, Marshall AJ, Hauch KD, Ratner BD, Fleckman P, Olerud JE. A mouse model to evaluate the interface between skin and a percutaneous device. J Biomed Mater Res A. 2007; 83:915–922. [PubMed: 17567856]
6. Karnovsky MJ. A formaldehyde-glutaraldehyde fixative of high osmolarity for use in electron microscopy. J Cell Biol. 1965; 27:137. Abstract.
7. Richardson KC, Jarett L, Finke EH. Embedding in epoxy resins for ultrathin sectioning in electron microscopy. Stain Technol. 1960; 35:313–323. [PubMed: 13741297]
8. Humason, G. Animal tissue techniques. San Francisco London: W. H. Freeman and Company; 1962.
9. O'Brien FJ, Harley BA, Yannas IV, Gibson LJ. The effect of pore size on cell adhesion in collagen-GAG scaffolds. Biomaterials. 2005; 26:433–441. [PubMed: 15275817]
10. Underwood RA, Usui ML, Zhao G, Hauch KD, Takeno MM, Ratner BD, Marshall AJ, Shi X, Olerud JE, Fleckman P. Quantifying the effect of pore size and surface treatment on epidermal incorporation into percutaneously implanted sphere-templated porous biomaterials in mice. J Biomed Mater Res A. 2011
11. Hall CW, Adams LM, Ghidoni JJ. Development of skin interfacing cannula. Trans Am Soc Artif Intern Organs. 1975; 21:281–288. [PubMed: 124976]
12. von Recum AF. Applications and failure modes of percutaneous devices: a review. J Biomed Mater Res. 1984; 18:323–336. [PubMed: 6234317]
13. Dovi JV, Szpaderska AM, DiPietro LA. Neutrophil function in the healing wound: adding insult to injury? Thromb Haemost. 2004; 92:275–280. [PubMed: 15269822]
14. Singer AJ, Clark RA. Cutaneous wound healing. N Engl J Med. 1999; 341:738–746. [PubMed: 10471461]
15. Martin P, Leibovich SJ. Inflammatory cells during wound repair: the good, the bad and the ugly. Trends Cell Biol. 2005; 15:599–607. [PubMed: 16202600]
16. Wetzler C, Kampfer H, Stallmeyer B, Pfeilschifter J, Frank S. Large and sustained induction of chemokines during impaired wound healing in the genetically diabetic mouse: prolonged persistence of neutrophils and macrophages during the late phase of repair. J Invest Dermatol. 2000; 115:245–253. [PubMed: 10951242]
17. Dovi JV, He LK, DiPietro LA. Accelerated wound closure in neutrophil-depleted mice. J Leukoc Biol. 2003; 73:448–455. [PubMed: 12660219]
18. Makela M, Larjava H, Pirila E, Maisi P, Salo T, Sorsa T, Uitto VJ. Matrix metalloproteinase 2 (gelatinase A) is related to migration of keratinocytes. Exp Cell Res. 1999; 251:67–78. [PubMed: 10438572]
19. Winter GD. Transcutaneous implants: reactions of the skin-implant interface. J Biomed Mater Res. 1974; 8:99–113. [PubMed: 4616966]
20. Gibran NS, Tamura R, Tsou R, Isik FF. Human dermal microvascular endothelial cells produce nerve growth factor: implications for wound repair. Shock. 2003; 19:127–130. [PubMed: 12578120]
21. Leon A, Buriani A, Dal Toso R, Fabris M, Romanello S, Aloe L, Levi-Montalcini R. Mast cells synthesize, store, and release nerve growth factor. Proc Natl Acad Sci U S A. 1994; 91:3739–3743. [PubMed: 8170980]
22. Akasaka Y, Ono I, Kamiya T, Ishikawa Y, Kinoshita T, Ishiguro S, Yokoo T, Imaizumi R, Inomata N, Fujita K, Akishima-Fukasawa Y, Uzuki M, Ito K, Ishii T. The mechanisms underlying fibroblast apoptosis regulated by growth factors during wound healing. J Pathol. 2010; 221:285–299. [PubMed: 20527022]
23. Martinez FO, Helming L, Gordon S. Alternative activation of macrophages: an immunologic functional perspective. Annu Rev Immunol. 2009; 27:451–483. [PubMed: 19105661]

24. Mahdavian Delavary B, van der Veer WM, van Egmond M, Niessen FB, Beelen RH. Macrophages in skin injury and repair. Immunobiology. 2011; 216:753–762. [PubMed: 21281986]
25. Moodley YP, Caterina P, Scaffidi AK, Misso NL, Papadimitriou JM, McAnulty RJ, Laurent GJ, Thompson PJ, Knight DA. Comparison of the morphological and biochemical changes in normal human lung fibroblasts and fibroblasts derived from lungs of patients with idiopathic pulmonary fibrosis during FasL-induced apoptosis. J Pathol. 2004; 202:486–495. [PubMed: 15095276]
26. Marshall AJ, Irvin CA, Barker T, Sage EH, Hauch KD, Ratner BD. Biomaterials with tightly controlled pore size that promote vascular in-growth. Polym. Preprints. 2004; 45:100–101.
27. Tavakkol Z, Samuelson D, deLancey Pulcini E, Underwood RA, Usui ML, Costerton JW, James GA, Olerud JE, Fleckman P. Resident bacterial flora in the skin of C57BL/6 mice housed under SPF conditions. J Am Assoc Lab Anim Sci. 2010; 49:588–591. [PubMed: 20858360]
28. Spenny ML, Muangman P, Sullivan SR, Bunnett NW, Ansel JC, Olerud JE, Gibran NS. Neutral endopeptidase inhibition in diabetic wound repair. Wound Repair Regen. 2002; 10:295–301. [PubMed: 12406165]
29. Sullivan S, Underwood R, Gibran N, Sigle RO, Usui M, Carter WG, JE O. Validation of a model for the study of multiple wounds in the diabetic mouse (db/db). Plast Reconstr Surg. 2004; 113:953–960. [PubMed: 15108888]
30. Sullivan SR, Underwood RA, Sigle RO, Fukano Y, Muffley LA, Usui ML, Gibran NS, Antezana MA, Carter WG, Olerud JE. Topical application of laminin-332 to diabetic mouse wounds. J Dermatol Sci. 2007; 48:177–188. [PubMed: 17719208]
31. Zhao G, Hochwalt PC, Usui ML, Underwood RA, Singh PK, James GA, Stewart PS, Fleckman P, Olerud JE. Delayed wound healing in diabetic (db/db) mice with Pseudomonas aeruginosa biofilm challenge: a model for the study of chronic wounds. Wound Repair Regen. 2010; 18:467–477. [PubMed: 20731798]
32. Greenhalgh DG, Sprugel KH, Murray MJ, Ross R. PDGF and FGF stimulate wound healing in the genetically diabetic mouse. Am J Pathol. 1990; 136:1235–1246. [PubMed: 2356856]
33. Faryniarz DA, Chaponnier C, Gabbiani G, Yannas IV, Spector M. Myofibroblasts in the healing lapine medial collateral ligament: possible mechanisms of contraction. J Orthop Res. 1996; 14:228–237. [PubMed: 8648500]

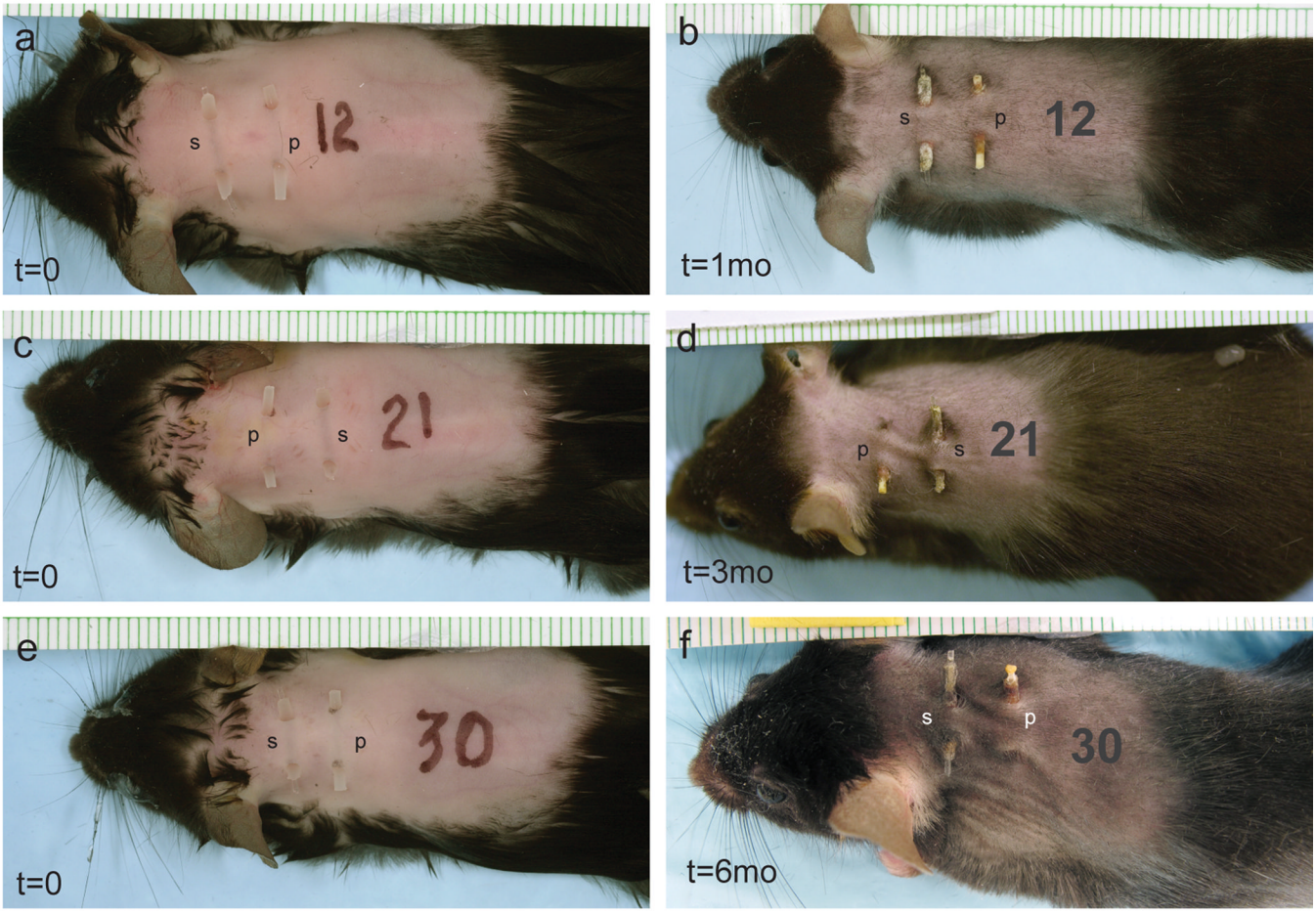

Figure 1.
Implants at time of implantation (a,c,e) and harvest (b,d,f). Mice in (a,c,e) were implanted at time=0 with both silicone (s) and poly(HEMA) (p) implants. Mice with implants in (b,d,f) are shown at time of harvest time, 1, 3 and 6 months, respectively.

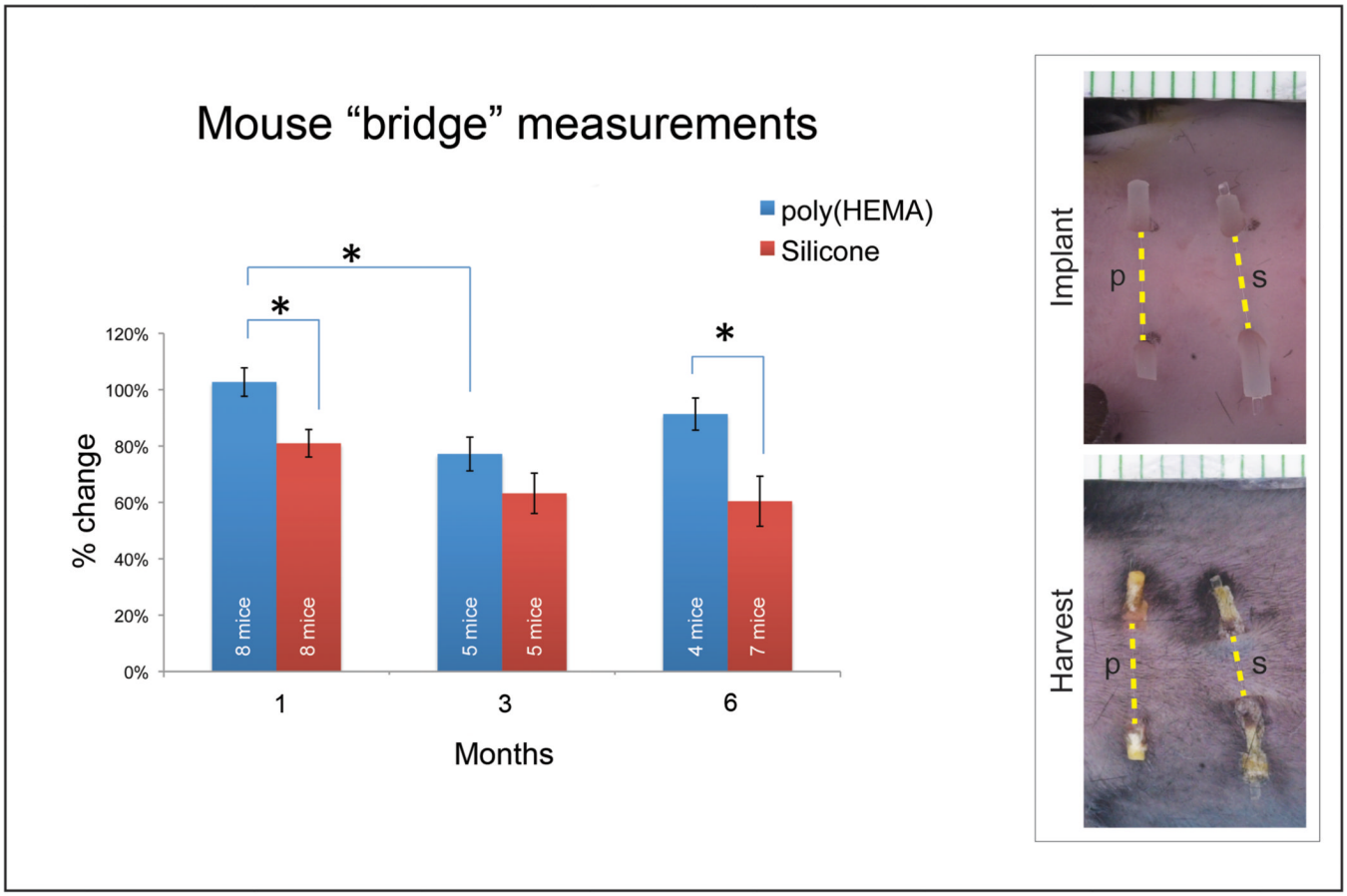

Figure 2.

Graph showing change in the length of skin that ‘bridges’ over the implant with time of implantation. Yellow dotted lines in macro photographs of a 1-month implant indicate measurements used for length calculation. Percent change in length of ‘bridge’ skin (distance between exit sites at harvest divided by distance between exit sites at implantation) was averaged for each harvest time point. Results are depicted in the graph for 1, 3 and 6 month implantations with 8, 5, and 4 mice evaluated for poly(HEMA) implants and 8, 5, and 7 mice evaluated for silicone implants, respectively. Bars indicate standard error with significance level* set at α=0.05.

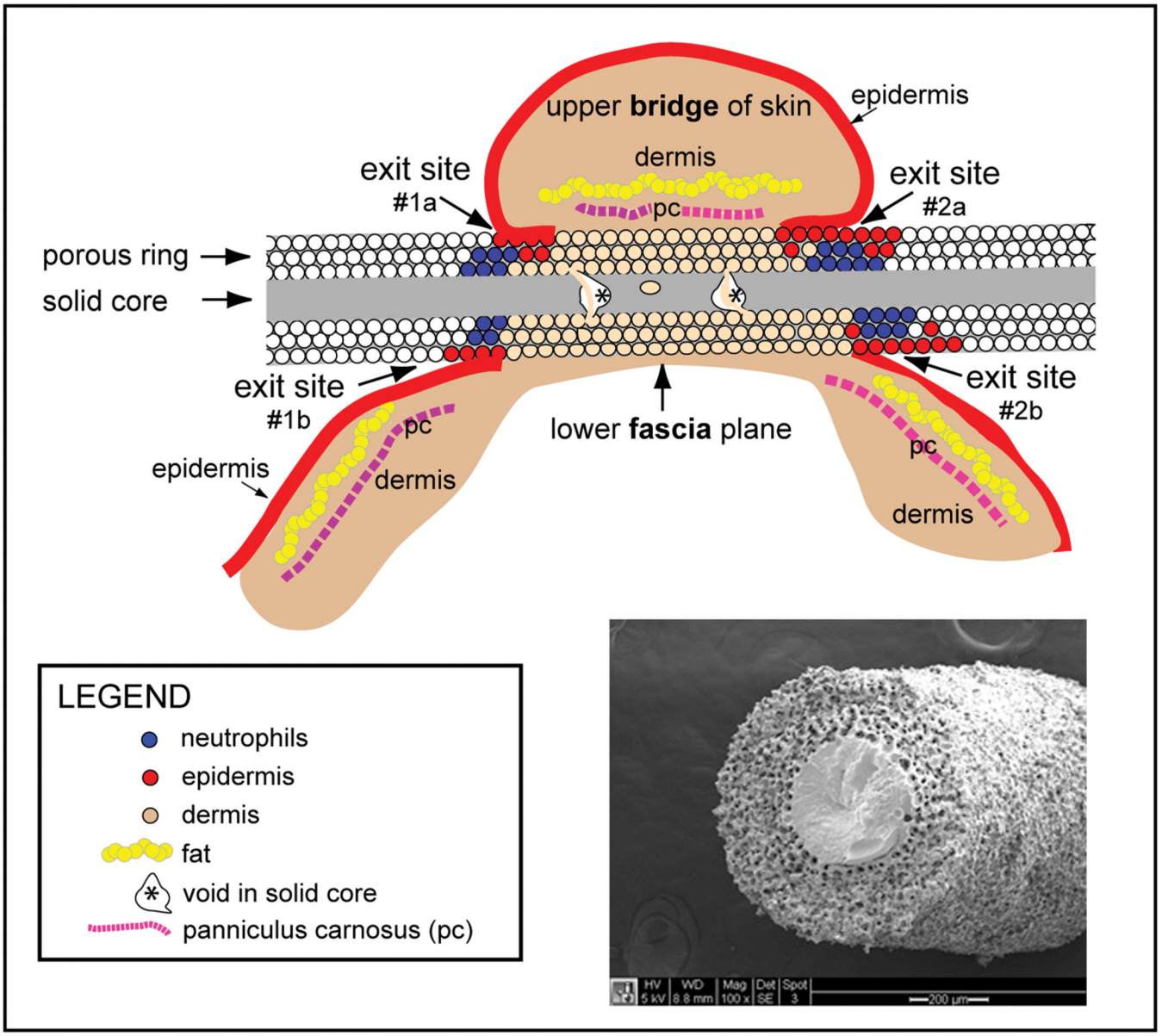

Figure 3.

Illustration of implant orientation in mouse skin and scanning electron micrograph of porous/solid poly(HEMA) rod. The illustration indicates orientation of the plane of sectioning for (immuno)histochemical analysis. Imperfections or breaks in the solid central core were termed “voids” (asterisks). SEM shows solid 0.4-mm diameter poly(HEMA) surrounded by porous poly(HEMA) with ~36 μm pores and ~14 μm interconnecting throats. Total O.D. is 1.2 mm.

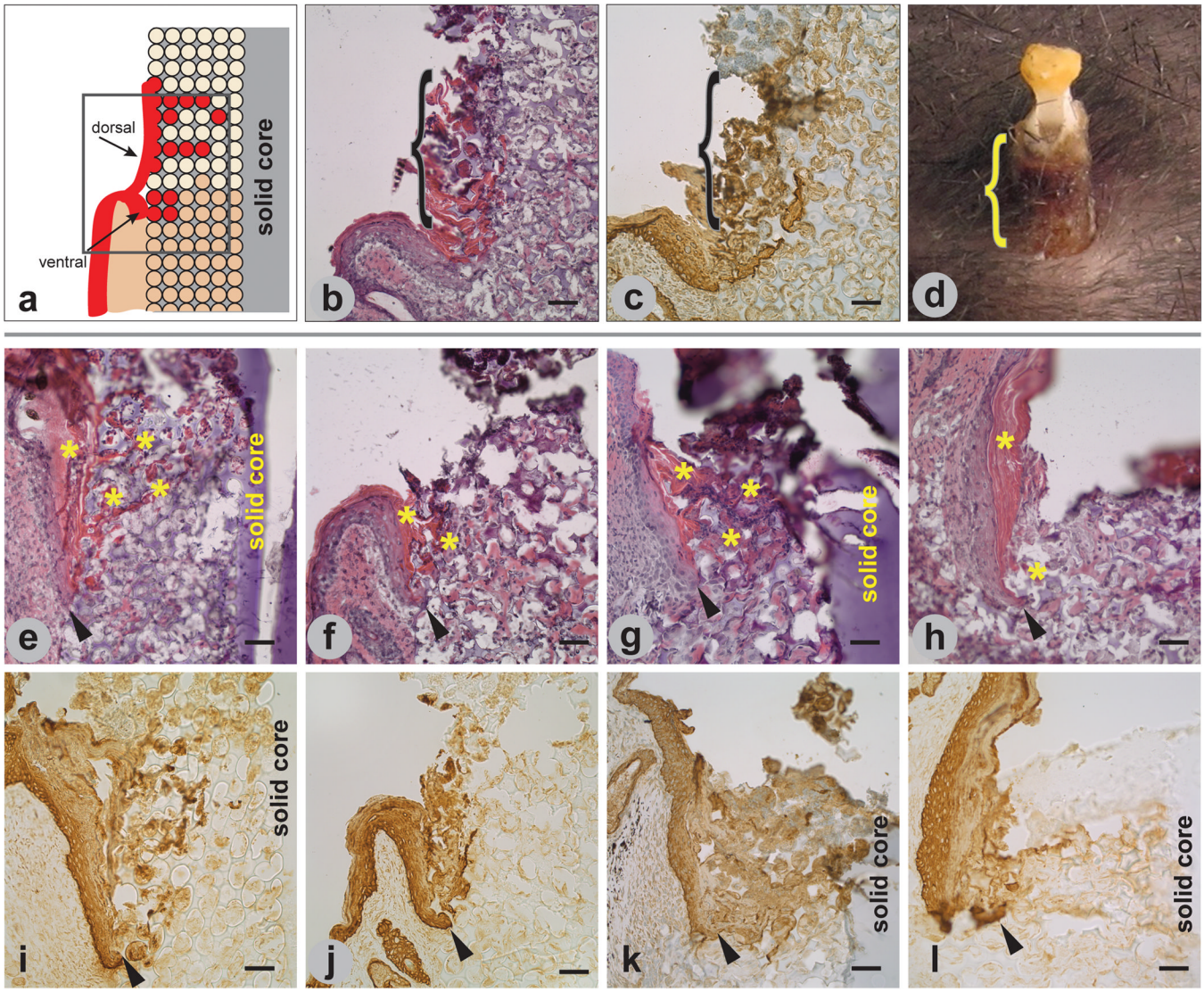

Figure 4.

Epidermal response to implanted porous/solid poly(HEMA). Illustration (a) of bifurcation of epidermis at the skin/implant interface showing keratinocytes (red) integrating into the pores from both the ventral and dorsal regions of the epidermis, with the dorsal region forming an epidermal sheath. H&E staining of implant/tissue section (b) showing cornified dorsal epidermis (pink) along and within the exterior region of a 1 1-month implant. Implant/tissue section in (c) is similar to the tissue section in (b) and immunostained with a pooled pankeratin and K14 antibody. Macro image of a 6-month implant in (d) shows external sheath formation. Brackets in (b–d) demarcate sheath. Tissue sections of 14-day (e,i), 1-month (f,j), 3-month (g,k), and 6-month (h,l) implants stained with H&E (e–h) and immunolabeled with pooled pankeratin and K14 antibody (i–l). Cornified dorsal epidermis (asterisks) is seen in (e–h). Arrowheads in (e–l) indicate tip of ventral migrating epidermis. Mag bars = 50 μm.

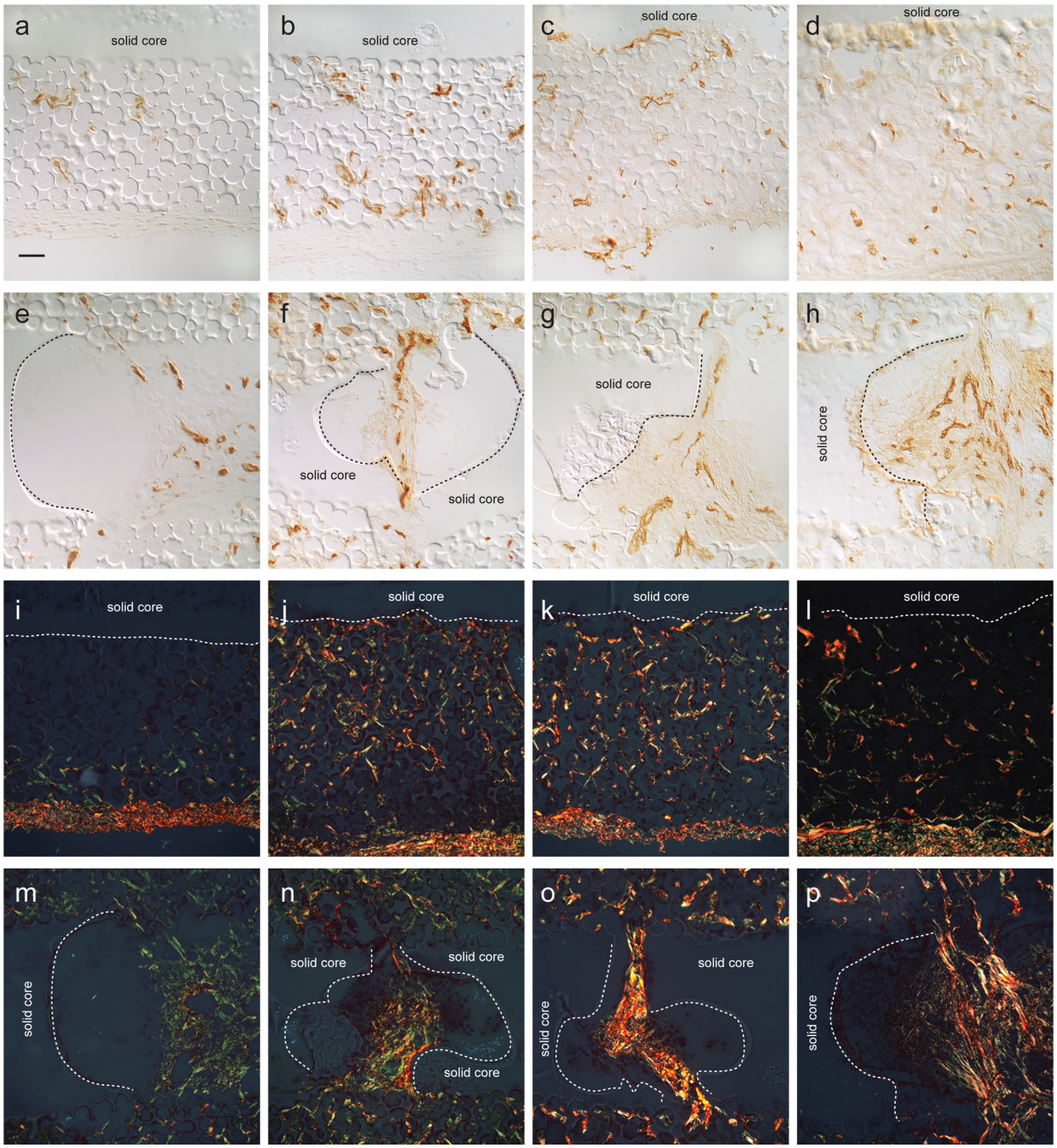

Figure 5.

PECAM-1 immunostaining and picrosirius red staining of 14-day (a,e,i,m), 1-month (b,f,j,n), 3-month (c,g,k,o), and 6-month (d,h,l,p) implant/tissue sections immunolabeled with PECAM-1(a–h) and stained with picrosirius red (i–p). Vessels appear to mature as a function of time (a–d). Voids in the solid region of the poly(HEMA) rod contiguous with the outer porous regions (e–h) show vessel maturation as a function of time. These vessels appeared to occupy the central regions of the voids. Implant/tissue sections stained with picrosirius red, using polarization to visualize collagen fibers (i–p) show finer collagen fibers (green) and larger collagen bundles. (yellow to red fibers). Collagen bundles appeared to mature with time (i–l).. Collagen fibers in the void regions (m–p) show collagen bundles

becoming more robust with time and occupying the central regions of the voids. Magnification is same for all images, with mag bar in (a) = 50μm. Dotted lines in (i–l) indicate porous/solid poly(HEMA) interface and in (m–p) indicate border of voids found in the solid poly(HEMA) core.

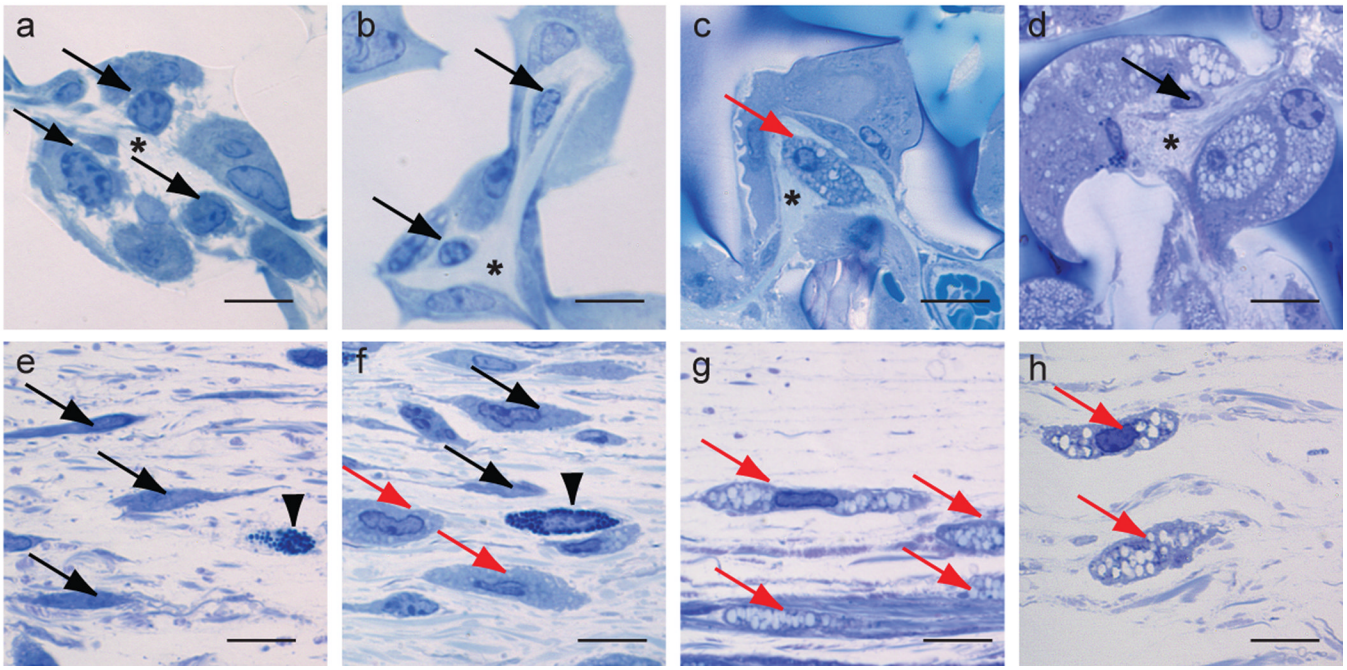

Figure 6.
Richardson's stained sections of 14-day (a,e), 1-month (b,f), 3-month (c,g) and 6-month (d,h) implants. Fibroblasts are shown within the pores (a–d) and in the fascia of the tissue surrounding the implants (e–g) (black arrows (non-vacuolated fibroblasts), red arrows (vacuolated fibroblasts). Arrowheads indicate mast cells, asterisks indicate collagen. Mag bar = 10 μm.

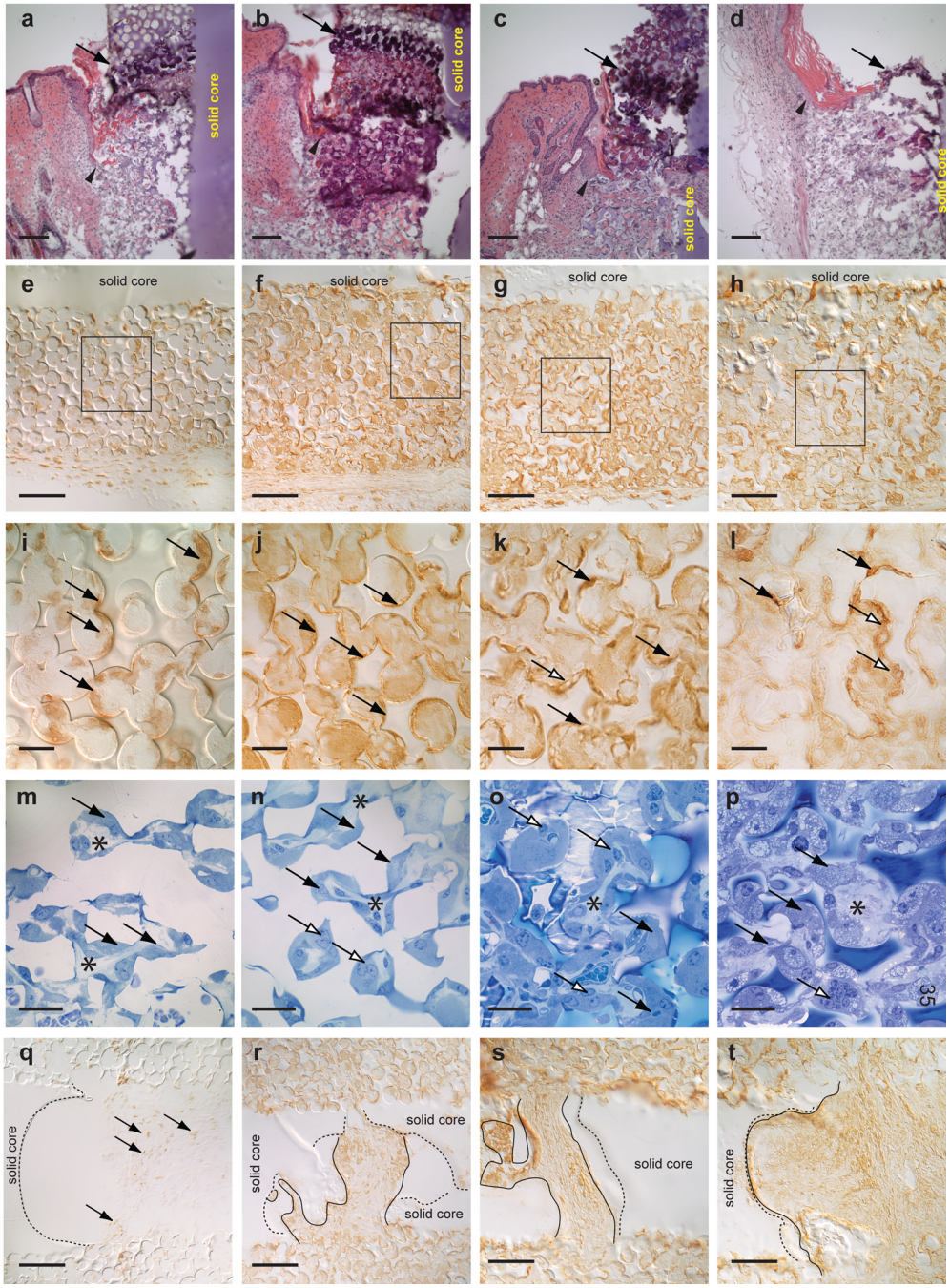

Figure 7.

Inflammatory response to implants. 14-day implants (a, e, i, m, q), 1-month implants (b, f, j, n, r), 3-month implants (c, g, k, o, s) and 6-month implants (d, h, l, p, t). H&E stained implant/tissue sections (a–d) showing dense neutrophil layer within the implant pores near the epidermal region (arrow). Tips of migrating epithelial tongue are identified by arrowheads. Implant/tissue sections in (e–l) immunostained with F4/80, a pan-macrophage antibody showing presence of macrophages lining poly(HEMA) pores. Higher magnification of boxed regions in (e–h) show macrophages (arrows) lining the concave surfaces of the pores in (i) and filling the pores in (j–k). The staining pattern in the 6-month implant (l) is much more amorphous. Tissue sections stained with Richardson's stain (m–p)

show morphological changes of the macrophages. The macrophages in the 3-month implants (o) appear to be bloated while the macrophages in the 6-month implant (p) appear to be highly vacuolated. The open arrows in (k, l, n, o, p) indicate macrophages possibly merging together to form multinucleated cells. F4/80 immunostained cells are found within the voids (q–r). Macrophages do not appear to line the inner wall of the voids in the solid core in the 14-day to 3-month implants (q–s) but are seen along the inner wall of the void in the 6-month implant (t). Black arrows in (i–q) indicate representative macrophages. Dotted lines in (q–t) indicate borders of voids found in the solid poly(HEMA) core. Solid lines in (r–t) indicate margins of F4/80 staining. Mag bars in panels (a–h, q–t) = 100 μm, in panels (i–p) = 25 μm.

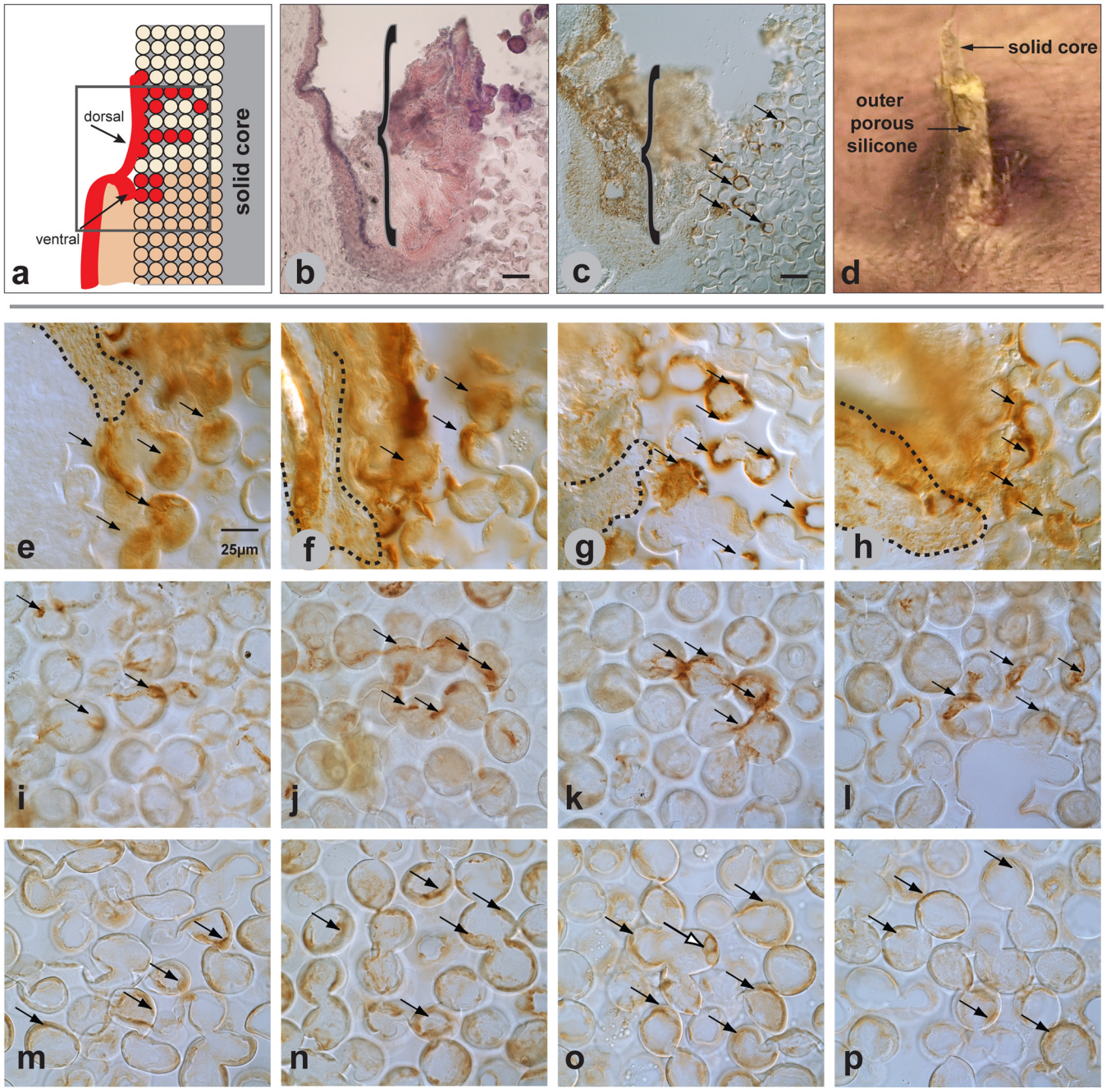

Figure 8.

Cutaneous response to implanted porous/solid silicone. Illustration of bifurcation of epidermis at the skin/implant interface (a) shows keratinocytes (red) integrating into the pores from both the ventral and dorsal regions of the epidermis with the dorsal region forming an epidermal sheath. H&E staining of implant/tissue section (b) shows cornified dorsal epidermis (pink) along and within the exterior (sheath) region of a 3-month silicone implant. Similar implant/tissue section as (b) immunolabeled with pooled pankeratin and K14 antibody (c) shows epidermal integration into the pores (arrows). Macro image of a 3-month implant in (d) shows the solid silicone rod surrounded by porous silicone. It is difficult to determine presence of an epidermal sheath in this image, although the tissue

sections in (b) and (c) demonstrate the presence of a sheath. Tissue sections of 14-day (e, i, m), 1-month (f, j,n), 3-month (g, k, o), and 6-month implants (h, l, p), immunolabeled with a pooled pankeratin and K14 antibody (e–h) show ventral keratinocytes appearing to migrate into the first 4–5 pores. Tissue sections immunolabeled with PECAM-1 antibody (i–l) show vessels present at all time points. Tissue sections immunolabeled with F4/80 antibody (m–p) show macrophages lining silicone pores at all time points. Mag bars in a–c = 50μm, Images e–p are the same magnification with mag bar shown in (e) = 25 μm.

Table 1

Integrity of implants as a function of time for each implant exit site used for each implant exit site. Number of exit sites/implant = 2.

	Evaluation of implant integrity at <u>each</u> exit site					
	poly(HEMA)			**silicone**		
Implant duration	Intact	Broken @ exit site	Covered with skin	Intact	Broken @ exit site	Covered with skin
14 days	16/16	0	0	16/16	0	0
1 mo	16/16	0	0	16/16	0	0
3 mo *	5/10	4/10	1/10	10/10	0	0
6 mo †	1/14	5/14	8/14	12/14	0	2/14

* Data represents results for 14 day, and 1, 3, and 6 month harvests for 8, 8, 5 and 7 mice, respectively.

* Only 5 mice were included for the 3 month harvest because confirming gross images for 3 mice could not be analyzed.

† One mouse for the 6 month harvest was euthanized early due to malocclusion of the teeth.